Ab initio study of structural, electronic and thermodynamic properties of tungstate double perovskites Ba_2MWO_6 (M = Mg, Ni, Zn)

O. Sahnoun [a,c,*], H. Bouhani-Benziane [a], M. Sahnoun [a], M. Driz [b], C. Daul [c]

[a] Laboratoire de Physique Quantique de la Matière et Modélisation Mathématique (LPQ3M), University of Mascara, Algeria
[b] Laboratoire de Sciences des Matériaux (LSM), University of Sidi Bel Abbes, Algeria
[c] Department of Chemistry, University of Fribourg, Switzerland

The structural and electronic properties of the double perovskite Ba_2MWO_6 with M = Mg, Ni, Zn have been studied using the full-potential linearized augmented plane wave (FP-LAPW) method by employing both the local density approximation (LDA) and the generalized gradient approximation (GGA), which are based on exchange–correlation energy optimization to calculate the total energy. Also we have used the Engel–Vosko GGA formalism, which optimizes the corresponding potential for band structure calculations. However, we have evaluated the ground state quantities such as lattice parameter, bulk modulus and its pressure derivative. Also, we have presented the results of the band structures and densities of states. These results were in favorable agreement with previous theoretical works and the existing experimental data. To complete the fundamental characteristics of these compounds we have analyzed the thermodynamic properties such as thermal expansion coefficient, heat capacities and other structural parameters in the whole pressure range from 0 to 20 GPa and temperature range from 0 to 1000 K.

1. Introduction

Because of their variable structure and composition, perovskite materials have attracted intense research interest in many applied and fundamental areas of solid-state science and advanced materials research at least for half a century. The perovskite structure (with general formula ABO_3) can be described as a framework of oxygen octahedral sharing corners [1,2]. The B-cations are located in the centers of octahedra and the interstitial sites are occupied by the A-cations. In complex perovskites two (or more) cations of different valences are located in the equivalent crystallographic positions [3]. Among the $A_2B'B''O_6$ complex perovskite oxides, where B′ and B″ are the cations of different valences, the mixed alkaline earth tungstate double perovskites with the general formula A_2BWO_6 (A = Ba, Sr, Ca; B = Mg, Co, Zn, Ni) are of interest for their complete 1:1 ordered state due to their larger differences in charge and ionic radii on B-site [4]. The barium containing tungstate double perovskites were determined to be cubic and in the space group Fm3m [5]. Ba_2MWO_6 (where M = Ni, Mg) have shown great potential as ceramic components for temperature sensors for example in petroleum wells [6]. These ceramics were produced by solid-state reaction process and sintered at different sintering conditions [7]. Understanding properties of these compounds and related materials at the atomistic level may help to improve the performance of their applications. Despite the recent progress in understanding the physics of the double perovskites there is still an open debate on the adequate theoretical modeling. In particular, the details of the interplay between structural, electronic, and magnetic degrees of freedom in the double perovskites are not yet clearly understood. To our knowledge, there is less or none theoretical studies in the literature devoted to electronic and thermal properties of mixed alkaline earth tungstate double perovskites.

The aim of this work is to provide information of some ordered tungstate double perovskites, and describes results for three of these, namely Ba_2MgWO_6, Ba_2NiWO_6 and Ba_2ZnWO_6. These particular compounds are reported to be cubic at room temperature [8], in contrast to many others which are somewhat distorted. The paper is organized as follows: in Section 2 we briefly describe the technical details of the employed methods for calculations. Section 3 presents and discusses the results of the electronic and thermodynamic properties. A summary concludes the paper in Section 4.

2. Computational details

The calculations presented in this work were performed using the FP-LAPW method, as implemented in the Wien2k code [9]. This method allows the inclusion of local orbital in the basis, improving upon linearization and making possible a consistent treatment of

* Corresponding author at: Laboratoire de Physique Quantique de la matière et Modélisation Mathématique (LPQ3M). University of Mascara, Algeria.
E-mail address: omar.sahnoun29@gmail.com (O. Sahnoun).

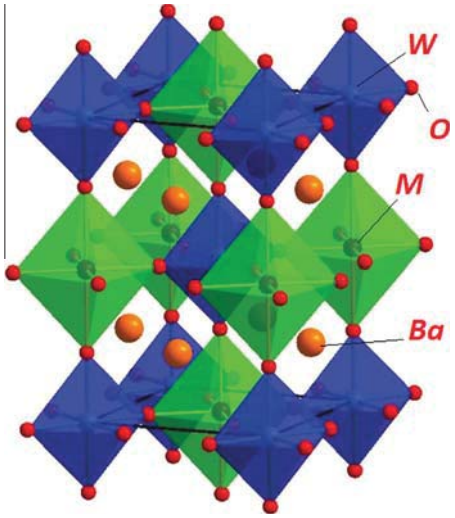

Fig. 1. The crystal structure of double perovskite Ba_2MWO_6.

semicore and valance states in an energy window, hence ensuring proper orthogonality. It is well known in the self-consistent band structure calculation within DFT [10], both LDA [11] and generalized gradient approximation (GGA) [12] usually underestimates the energy gap [13]. This is mainly due to the fact that they have simple forms that are not sufficiently flexible to accurately reproduce both the exchange–correlation energy and its charge derivative. Engel and Vosko considered this shortcoming and constructed a new functional form of GGA [14] which is able to better reproduce the exchange potential at the expense of less agreement in the exchange energy. This approach called EV-GGA yields better band splitting and some other properties which mainly depend on the accuracy of exchange–correlation potential.

All the calculations were converged with respect to Brillouin zone (BZ) sampling and the size of the basis set. Brillouin zone (BZ) integrations within the self-consistency cycles were performed via a tetrahedron method, using $8 \times 8 \times 8$ special k-points mesh [15]. The convergence parameter $R_{mt}K_{max}$, which controls the size of the basis sets, was set to 8. The G_{max} parameter was taken to be 12 $Bohr^{-1}$. The muffin-tin radii were taken as (2.5, 1.8, 1.6, 2.0, 2.0, 1.98) a.u. for (Ba, W, O, Mg, Ni, Zn), respectively. Careful convergence tests show that with these parameters relative energy converged to better than 10^{-5} Ry per formula unit.

3. Results and discussion

3.1. Structural properties

We employed the experimentally observed cubic crystalline structures [16] for the three compounds in the calculation, which can be described by the space group Fm3m, with Ba ions in 8(c) positions at 1/4, 1/4, 1/4; M (M = Mg, Ni or Zn) in 4(a) at 0,0,0; W in 4(b) at 1/2, 1/2, 1/2; and O in 24(e) at x,0,0. In the ordered cubic double perovskites Ba_2MWO_6 (M = Mg, Ni or Zn), the M and W cations are octahedrally coordinated by oxygen anions (see Fig. 1). In this aristotype cubic structure, the highly electropositive Ba cation is coordinated to 12 oxygens, while each M cation has 6 W cations as nearest neighbors and vice versa. With this arrangement the intermediate oxygen anions can satisfy the different bond length requirements of the two cations by moving toward the smaller ion. This structure is often viewed in terms of an ordered alternation of M and W cation layers perpendicular to the [1 1 1] direction. The lattice parameters, the bulk moduli and the oxygen parameter x which can deviate from the ideal value of 0.25 realized in the simple perovskite structure, are summarized in Table 1, together with the available experimental [17–21] and other theoretical calculation data [22–26]. It can be seen that calculated lattice constants are overestimated with the experimental data not more than 1%, which indicates that the present calculations are highly reliable. In the current work, the bulk modulus is in reasonable agreement with other theoretical calculations in the case of Ba_2MgWO_6.

3.2. Electronic properties

All electronic properties have been calculated for the equilibrium geometry. We collected data on the optical gaps in Table 2. In Fig. 2 we presented the band structures for each crystal calculated using the Engel–Vosko GGA formalism. It can be seen from Fig. 2 that the conduction band (CB) structure is nearly unaffected by the different B-cations in the lattice while the top of valence band (VB) increases inducing an obvious band gap narrowing. The bottom of the conduction band lies at the X-point in all three double-perovskite crystals. The electron energy in the lowest conduction band at the X-point is just 0.7–1.3 eV higher than at the bottom of conduction bands. So, there is a little dispersion in the lowest conduction band between the W, L and X points in the Brillouin zone. The top of the valence band is displaced from the L point of the Brillouin zone in Ba_2NiWO_6 and Ba_2ZnWO_6 to the Γ-point in Ba_2MgWO_6. The highest valence electron states at the Γ-point appear only about 0.05 eV below the highest states in X-point for both Ba_2MgWO_6 and Ba_2ZnWO_6 compounds. The dispersion of the top valence band is almost flat between Γ and X points for these two compounds. The additional d-orbitals on Zn ions in Ba_2ZnWO_6 cause the appearance of an additional valence band below the other bands. They cause also the highest states at the Γ-point to rise above all other valence states and to make a new top of the valence band. The effect of the electronic structure perturbation caused by different B-cations located in the centers of octahedra is illustrated by a comparison of the total and projected densities of states (DOSs) for the three compounds Ba_2MgWO_6, Ba_2NiWO_6 and Ba_2ZnWO_6. From Fig. 3, we can find that the DOS can be mainly divided into four parts. The first part extending from −11 to −9.5 eV is characterized by a peak mainly due to the contribution of Ba ions. On the other hand, near the Fermi level (E_F) until

Table 1
Summary of calculated lattice constants (Å), the oxygen parameter x, and bulk modulus (GPa) of Ba_2MgWO_6, Ba_2NiWO_6 and Ba_2ZnWO_6 at zero pressure, compared with experimental and other theoretical data.

	a (Å)	B (GPa)	B′	x
Ba_2MgWO_6				
LDA	8.016	187.78	4.44	0.259
GGA	8.095	175.87	4.65	0.261
Exp. [17]	8.1345	137.00	3.90	0.241
Exp. [18]	8.112			
Exp. [19]	8.1046			
Cal. [22]	8.099			
Cal. [23]	8.0166	149.67	4.51	0.239
Ba_2NiWO_6				
LDA	7.943	201.86	4.69	0.258
GGA	8.032	187.22	4.70	0.259
Exp. [20]	8.060			0.260
Exp. [21]	8.066			
Cal. [24]	8.064			
Ba_2ZnWO_6				
LDA	8.023	193.78	4.70	0.261
GGA	8.110	180.15	4.50	0.262
Exp. [19]	8.1362			
Exp. [21]	8.1216			
Cal. [24]	8.137			
Cal. [25]				0.236
Cal. [26]				0.237

Table 2
Summary of calculated band gaps (eV) compared with experimental and other theoretical data.

Band gap	EV-GGA	LDA	GGA	Exp.	Cal.
Ba_2MgWO_6					
Γ–Γ	3.316	2.515	2.450		
X–X	3.056	2.412	2.303		
W–W	4.017	3.214	3.265		
L–L	4.038	3.204	3.289		
L–X	3.400	2.706	2.749		
Γ–X	3.000	2.349	2.303	3.4 [28] 3.5 [29]	2.89 [28,23]
Ba_2NiWO_6					
Γ–Γ	3.609	2.833	3.019		
X–X	2.970	2.350	2.528		
W–W	3.048	2.041	2.283		
L–L	2.450	1.520	1.758		
L–X	2.204	2.870	1.562		
Γ–X	3.265	2.586	2.823		
Ba_2ZnWO_6					
Γ–Γ	3.633	2.589	3.658		
X–X	3.404	2.588	3.300		
W–W	4.173	3.126	4.130		
L–L	3.530	2.476	3.457		
L–X	3.064	2.144	3.000	3.5 [28] 3.8 [29]	
Γ–X	3.314	2.423	3.274		

−5.7 eV for $Ba_2(Mg,Zn)WO_6$ and −7 eV for Ba_2NiWO_6, consists predominantly of oxygen (O) ion, but contains a small admixture of Mg, Ni, and Zn and W ions. The oxygen p-orbitals give the primary contribution to the valence band of all three studied perovskites. These O 2p-orbitals are perpendicular to the W–O–M (M = Mg, Ni, Zn) bridge and lie in the BaO-planes. The additional valence bands contain contributions mostly from W 6s-orbitals. These orbitals contribute to the valence bands through the entire set of the bands. In the conduction band both the oxygen (O) and tungsten (W) ions contribute to roughly the same amount, which is extending from 3.10 to 4.30 eV for $Ba_2(Mg,Zn)WO_6$ and 2.30 to 3.20 eV for Ba_2NiWO_6. Last part, at higher energies of the conduction band, consists of Ba, Mg, W, and O ions, but a small from Ni, Zn. From Fig. 3, it can be found that the PDOS of Ba and W atoms have almost the same contribution to DOS for the three compounds Ba_2MgWO_6, Ba_2NiWO_6 and Ba_2ZnWO_6. Many of the W 5d states are empty and located above E_F, while also a few states occupy the region below E_F due to the strong hybridization with oxygen. The optical band gaps of the three double-perovskites obtained using different functionals are summarized in Table 2. This table clearly demonstrates that both LDA and GGA calculations dramatically underestimate the optical gap by several times for all three perovskites. This tendency is well known in solid state physics [27]. The most realistic band gaps have been obtained using the Engel–Vosko GGA functional, in agreement with avail-

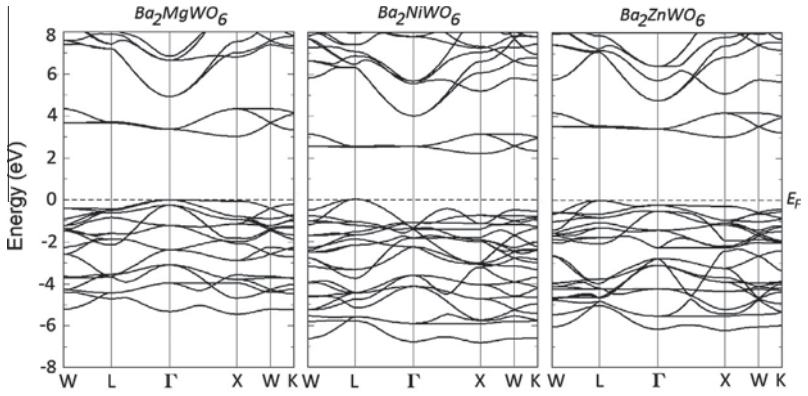

Fig. 2. Calculated band structures of (a) Ba_2MgWO_6, (b) Ba_2NiWO_6 and (c) Ba_2ZnWO_6.

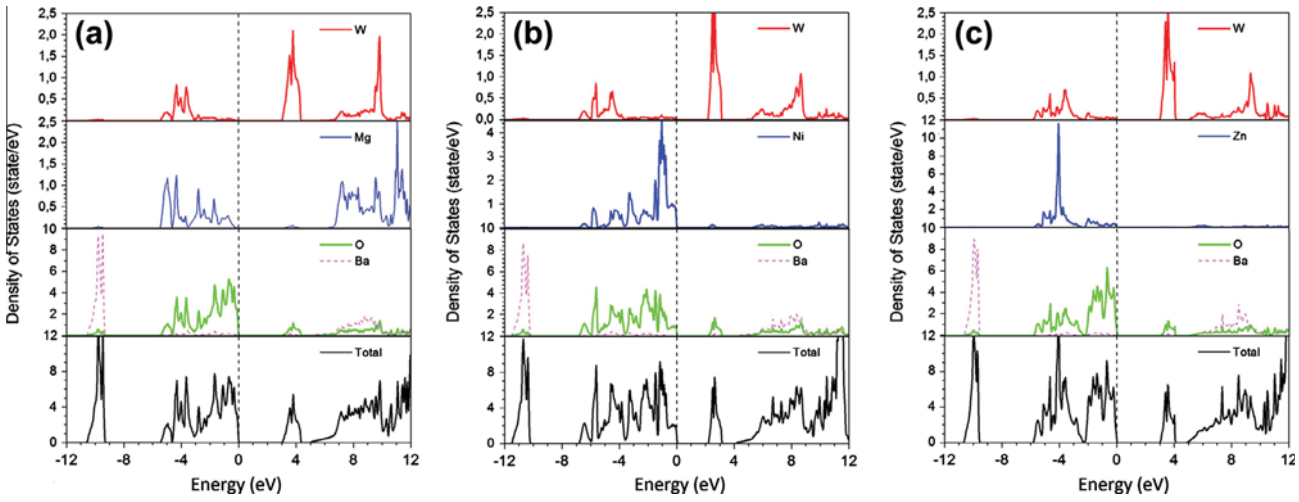

Fig. 3. Calculated partial density of states and total density of states of (a) Ba_2MgWO_6, (b) Ba_2NiWO_6 and (c) Ba_2ZnWO_6.

able studies. The Ba_2MgWO_6 experimental band gap is 3.4 eV (indirect gap), as determined by Eng et al. using the UV–visible diffuse reflectance spectroscopy [28], 3.5 eV band gap has also been measured for Ba_2ZnWO_6 [29]. In our calculations using the Engel–Vosko GGA functional, we have obtained the Ba_2MgWO_6 indirect band gap (Γ–X) of 3.06 eV. The value of 2.20 eV has been obtained for the indirect band gap (L–X) of Ba_2NiWO_6 and the value of 3.068 eV for the Ba_2ZnWO_6 indirect band gap (L–X). Our band gaps are in a good agreement with the experiment, the discrepancy is less than 10%. This is acceptable if we take into account difficulties in determining experimentally the band gap, including the optical absorption edge tails which extend up to several tenths of eV.

3.3. Thermodynamic properties

The thermal properties are determined by using a quasi-harmonic Debye, in which the non-equilibrium Gibbs function $G^*(V; P, T)$ is written in the form:

$$G^*(V;P,T) = E(V) + PV + F_{vib}[\Theta(V);T] \tag{1}$$

where $E(V)$ is the total energy per unit cell, PV corresponds to the constant hydrostatic pressure condition, $\Theta(V)$ is the Debye temperature and A_{vib} is the vibrational term which can be written using the Debye model of the phonon density of states as:

$$F_{vib}[\Theta(V);T] = Nk_BT\left[\frac{9\Theta}{8T} + 3\ln\left(1 - e^{-\frac{\Theta}{T}}\right) - D\left(\frac{\Theta}{T}\right)\right] \tag{2}$$

where $D(\Theta/T)$ represents the Debye integral, N the number of atoms in a chemical formula. Using a quasi-harmonic Debye model in the Slater formulation, the Debye temperatures $\Theta_D(V)$ are computed from the static bulk moduli $B_S(V)$, and the Poisson ratio is assumed to be volume independent, and equal to 1/4, corresponding to a Cauchy solid. This method, implemented in the GIBBS code and described with detail in Ref. [30], requires only a collection of $\{V, E(V)\}$ points around the equilibrium geometry. Assuming isotropic conditions, with Poisson ratio ν, Θ_D can be given by [30,31]:

$$\Theta_D = \frac{h}{k_B}\left[6\pi^2V^{1/2}N\right]^{1/3} f(\nu)\sqrt{\frac{B_S}{M}} \tag{3}$$

where M is the molecular mass per formula unit, and $f(\nu)$ is given by:

$$f(\nu) = \left\{3\left[2\left(\frac{2}{3}\frac{1+\nu}{1-2\nu}\right)^{3/2} + \left(\frac{1}{3}\frac{1+\nu}{1-\nu}\right)^{3/2}\right]^{-1}\right\}^{1/3} \tag{4}$$

The static bulk modulus is given by the curvature of the $E(V)$ function:

$$B_S \cong B_{static} = V\left(\frac{d^2E(V)}{dV^2}\right) \tag{5}$$

The curvature of the $E(V)$ function changes with the volume, increasing sharply as the crystal volume decreases, and decreasing in a lesser amount as the crystal expands. This asymmetry between the curvature at the left and at the right of the equilibrium volume is the origin of the volume dependence of Θ_D and it is the main reason behind the capability of the quasi-harmonic Debye model to predict the low temperature behavior of the crystal, including the $V(T)$ dependency. Accordingly, the non-equilibrium Gibbs function $G^*(V; P, T)$ as a function of V, P and T can be minimized with respect to volume V:

$$\left[\frac{\partial G^*(V;P,T)}{\partial V}\right]_{P,T} = 0 \tag{6}$$

By solving Eq. (6), one can obtain the thermal equation-of-state (EOS) $V(P, T)$. The heat capacity at constant volume C_V, the thermal expansion coefficient α, and the heat capacity at constant pressure C_P, are given respectively by [30]:

$$C_V = C_V(V(p,T),T) = \left(\frac{\partial G^*}{\partial T}\right)_V = 3Nk_B\left[4D\left(\frac{\Theta}{T}\right) - \frac{3\Theta/T}{e^{\Theta/T}-1}\right] \tag{7}$$

$$\alpha = \frac{\gamma C_V}{B_T V} \tag{8}$$

B_T is the isothermal bulk modulus given by:

$$B_T = -V\left(\frac{\partial p}{\partial V}\right)_T = V\left(\frac{\partial^2 F_{vib}}{\partial V^2}\right)_T \tag{9}$$

$$C_P = C_V(1 + \gamma\alpha T) \tag{10}$$

where γ is the Grüneisen parameter which is approximated as [32]:

$$\gamma = -\frac{d\ln(\Theta(V))}{d\ln V} \tag{11}$$

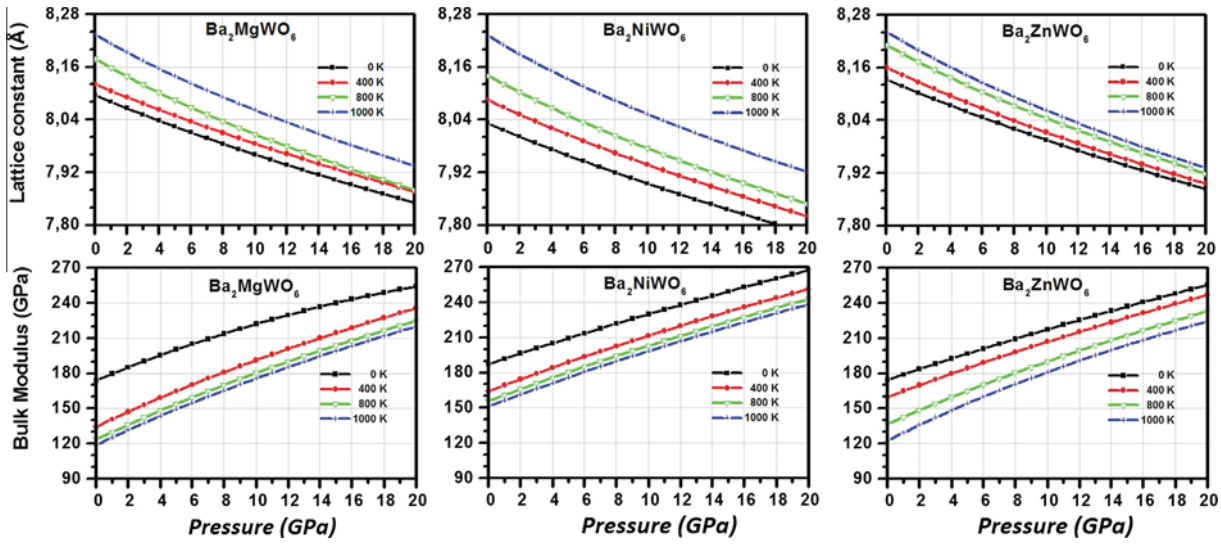

Fig. 4. The relationship between (a) lattice constants and (b) bulk modulus with pressure at temperatures of 0 K, 400 K, 800 K, and 1000 K, respectively.

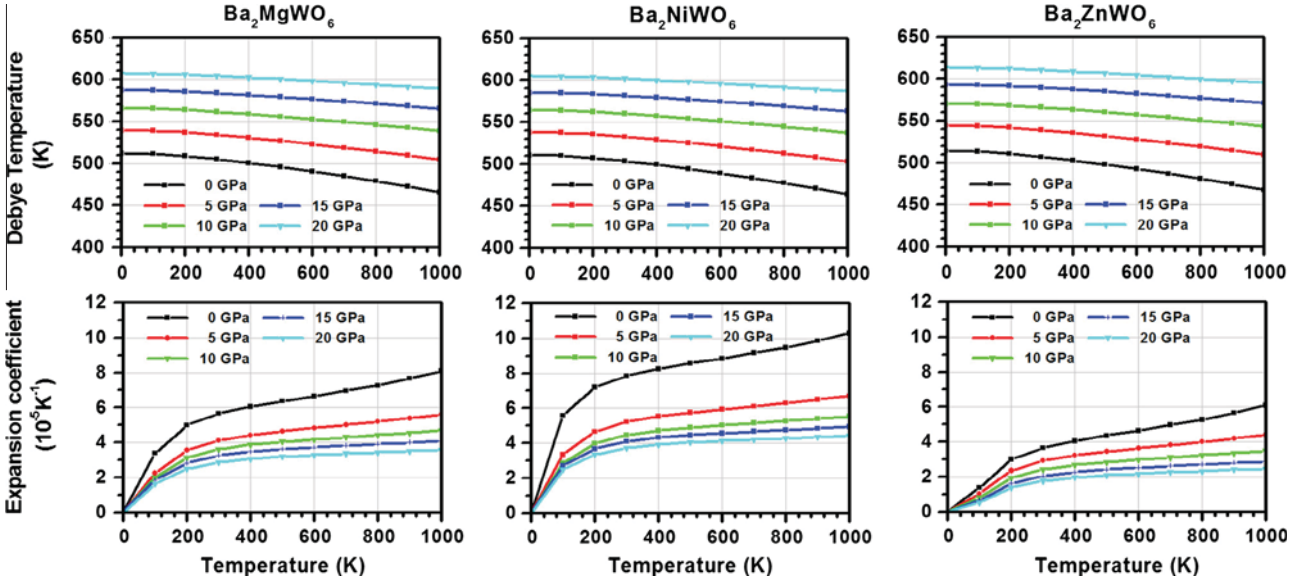

Fig. 5. Pressure and temperature dependence of (a) Debye temperature and (b) thermal expansion coefficient of Ba_2MgWO_6, Ba_2NiWO_6 and Ba_2ZnWO_6.

γ is calculated using a fit to entropy values at very low but not zero temperatures, for any volume. The thermal properties are determined in the temperature range from 0 to 1000 K, where the quasi-harmonic model remains fully valid. The pressure effect is studied in the 0–20 GPa range. The temperature effects on the lattice parameters are shown in Fig. 4. The lattice parameter increases with increasing temperature but the rate of increase is very moderate. It is also noted from the regular spacing of the curves in Fig. 4 that the relationships between bulk modulus and pressure are all nearly linear at various temperatures of 0, 200, 400, 600, 800 and 1000 K, respectively. The bulk modulus increases with pressure at a given temperature. However, the effect of increasing pressure on the material is the same as decreasing temperature of the material.

The calculated heat capacity at constant pressure C_P and heat capacity at constant volume C_V with the temperature T at different pressure P are shown in Fig. 5. The changing trends of the heat capacity of the three double-perovskite structures are similar. The difference between C_P and C_V is very small at low temperatures. However, at high temperatures, the C_V approaches a constant value, C_P increases monotonously with increments of the temperature. The values follow the Debye model at low temperature ($C_V(T) \propto T^3$), this is because only the long wavelength vibration modes of the lattice are populated and these modes could be approximated by treating the lattice as a continuum. However, the classical behavior ($C_V(T) \propto 3R$ for mono-atomic solids) is found at sufficient high temperatures, which is in agreement with the law of Petit and Dulong [33]. From Fig. 5, one can also see that the heat capacity increases with the temperature at the same pressure and decreases with the pressure at the same temperature, the influences of the temperature on the heat capacity are much more significant than that of the pressure on it.

The Debye temperature is the key quantity in the quasi-harmonic Debye model, which correlates with many physical

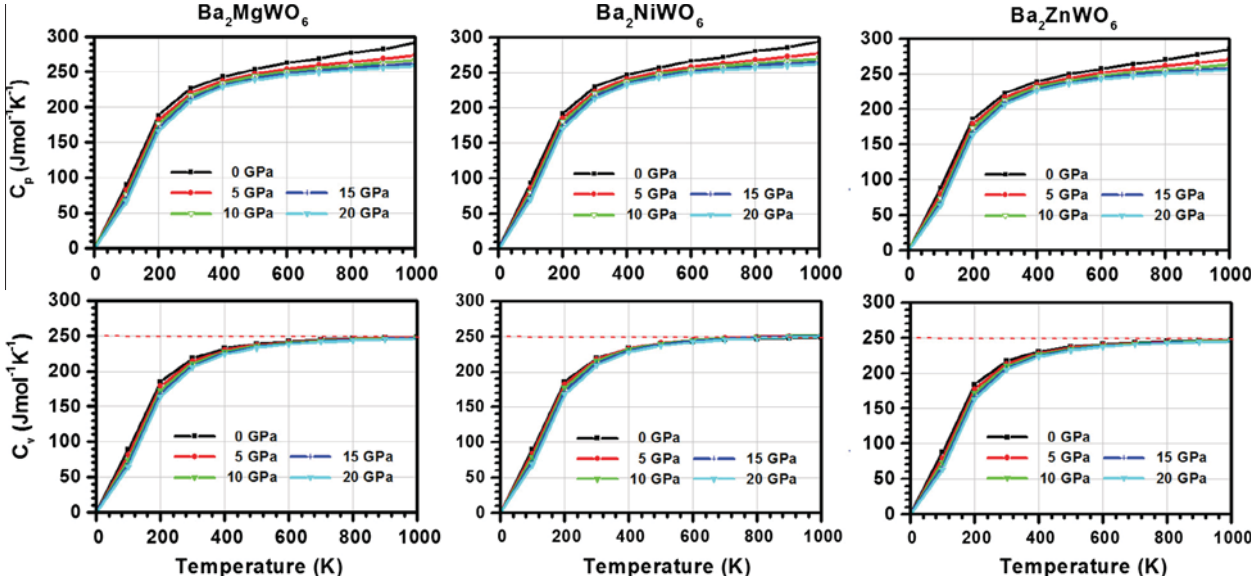

Fig. 6. Temperature dependence of (a) constant pressure heat capacity (C_p) and (b) constant volume heat capacity (C_v) of Ba_2MgWO_6, Ba_2NiWO_6 and Ba_2ZnWO_6.

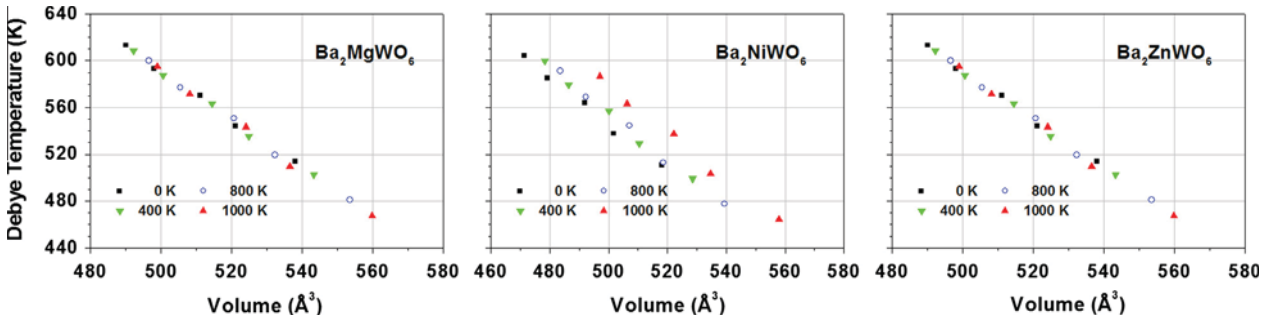

Fig. 7. Volume and temperature dependence of Debye temperature of Ba_2MgWO_6, Ba_2NiWO_6 and Ba_2ZnWO_6.

properties of solids, such as specific heat, elastic constants and melting temperature. We calculate dependence of the Debye temperature on pressure and temperature as shown in Fig. 6. The calculated value of Debye temperature at 0 K and 0 GPa is 512.58 K, 510.20 K, 515.20 K, for Ba_2MgWO_6, Ba_2NiWO_6 and Ba_2ZnWO_6, respectively. When the external pressure changes from 0 to 20 GPa, the calculated Debye temperature increases by (18.32%, 18.57%, 19.20%) and (26.13%, 26.60%, 27.48%) at temperatures of 0 and 1000 K, for all the three compounds, respectively. Additionally, it is seen in Fig. 6 that the Debye temperature decreases with temperature at a constant pressure and at a constant temperature it follows an almost linear relationship with pressure.

The variation of the thermal expansion coefficient with the pressures and temperatures can be seen in Fig. 6. It is clear that the temperature dependence of the thermal expansion coefficients of the three compounds follows a T^3 law for low temperature, and gradually increases linearly with the increment of temperatures. The effects of the pressure on the thermal expansion coefficients are very small at low temperatures; the effects are increasingly obvious as the temperature increases. As pressure increases, the thermal expansion coefficient decreases rapidly and the effects of temperature become less and less pronounced, resulting in linear high temperature behavior. It is noted that the high temperature dependence of the thermal expansion coefficient is not linearly at low pressure, this is an indication of the inadequacy of the quasi-harmonic approximation at high temperatures and low pressures.

Additionally, Fig. 7 illustrates certain systematic trends existing for the studied group of compounds. There is a linear and monotonic decrease of the Debye temperature with increasing the unit cell volume, at various temperatures. Such a trend was also reported earlier for the transition metal monocarbides [34]. These results can serve as the first predictions to be checked out by future works.

4. Conclusion

In this work, the structural and electronic properties of the Ba_2MgWO_6, Ba_2NiWO_6 and Ba_2ZnWO_6 compounds were investigated using first-principles calculations based on density functional theory. The calculated structural parameters obtained are consistent with the experimental data and other theoretical results. Density of states and electronic band structure often provide sufficient information for a through characterization of the electronic properties of a material. The energy band structure, total and partial density of states (DOSs) of the three compounds were calculated by FP-LAPW method. Our band gaps are in a good agreement with previous theoretical works and the existing experimental data, the discrepancy is found less than 10%. Temperature-dependent thermodynamic properties of Ba_2MgWO_6, Ba_2NiWO_6 and Ba_2ZnWO_6, including thermal expansion coefficient, bulk modulus, and heat capacity, have also been studied in terms of first-principles calculations and quasi-harmonic approach, wherein the thermal electronic and vibrational contributions are considered.

Acknowledgments

This work was supported by the Swiss National Science Foundation (NSF) and by the International Relations Office at the University of Fribourg.

References

[1] T. Kimura, Y. Tokura, Ann. Rev. Mater. Sci. 30 (2000) 451.
[2] F. Litchenberg, A. Herrnberger, K. Weidenman, J. Mannhart, Prog. Solid State Chem. 29 (2001) 1.
[3] S.G. Steward, H.P. Rooksby, Acta Crystallogr. 4 (1951) 503.
[4] M.T. Anderson, K.B. Greenwood, G.A. Taylor, Prog. Solid State 22 (1993) 197.
[5] D.D. Khalyavin, Jiaping Han, A.M.R. Senos, P.Q. Mantas, J. Mater. Res. 18 (2003) 2600.
[6] L. Salgado, F.A. Filho, Mater. Sci. Forum 448 (2008) 591.
[7] L.A. Rangel de Aguiar, C.M. Lapa, R.A.F. Sanguinetti, J.A. Aguiar, C.L. da Silva, D.P.F. Souza, Y.P. Yadava, Mater. Sci. Forum 523 (2005) 498.
[8] L.H. Brixner, J. Phys. Chem. 64 (1960) 165.
[9] P. Blaha, K. Schwarz, G.K.H. Madsen, D. Kvasnicka, J. Luitz, WIEN2k. An Augmented Plane Wave Plus Local Orbitals Program for Calculating Crystal Properties, Vienna University of Technology, Vienna, Austria, 2001.
[10] P. Hohenberg, W. Kohn, Phys. Rev. 136 (1964) 86.
[11] D.M. Ceperley, B.I. Ader, Phys. Rev. Lett. 45 (1980) 566.
[12] J.P. Perdew, S. Burke, M. Ernzerhof, Phys. Rev. Lett. 77 (1996) 3865.
[13] P. Dufek, P. Blaha, K. Schwarz, Phys. Rev. B 50 (1994) 7279.
[14] E. Engel, S.H. Vosko, Phys. Rev. B 47 (1993) 13164.
[15] H.J. Monkhorst, J.D. Park, Phys. Rev. B 13 (1976) 5188.
[16] C.N.R. Rao, Perovskites – Encyclopedia of Physical Science and Technology, third ed., 2003, pp. 707–714.
[17] S. Meenakshi, V. Vijayakumar, S.N. Achary, A.K. Tyagi, J. Phys. Chem. Solids 72 (2011) 609.
[18] V.S. Filipev, G.E. Shatalova, E.G. Fesenko, Kristallografiya 19 (1974) 386.
[19] D.D. Khalyavin, J. Han, A.M.R. Senos, P.Q. Mantas, J. Mater. Res. 18 (2003) 2600.
[20] D.E. Cox, G. Shirane, B.C. Fraze, J. Appl. Phys. 38 (1967) 1459.
[21] H. Iwakura, H. Einaga, Y. Teraoka, J. Nov. Carbohydr. Res. Sci. 3 (2011) 1.
[22] D.D. Khalayavin, J. HangSenos, A.M.R. Senos, P.Q. Mantas, J. Mater. Res. 18 (2003) 2600.
[23] M.G. Brik, J. Phys. Chem. Solids 73 (2012) 252.
[24] S. Dimitrovska, S. Aleksovska, I. Kuzmanovski, Cent. Eur. J. Chem. 198 (2005) 215.
[25] H.W. Eng, P.W. Barnes, B.M. Auer, P.M. Woodward, J. Solid State Chem. 175 (2003) 94.
[26] I.N. Belyaev, V.S. Filipev, E.G. Fesenko, Z. Strukt. Khim. 4 (1963) 719.
[27] L.J. Sham, M. Schluter, Phys. Rev. Lett. 51 (1983) 1888.
[28] H.W. Eng, P.W. Barnes, B.M. Auer, P.M. Woodward, J. Solid State Chem. 175 (2003) 94.
[29] B.E. Day et al., J. Solid State Chem. 185 (2012) 107.
[30] A. Otero-de-la-Roza, D. Abbasi-Pérez, V. Luaña, Comput. Phys. Commun. 182 (2011) 2232.
[31] A. Otero-de-la-Roza, V. Luaña, Comput. Theor. Chem. 975 (2011) 111;
A. Otero-de-la-Roza, V. Luaña, Phys. Rev. B 84 (2011) 024109.
[32] J.-P. Poirier, Introduction to the Physics of the Earth's Interior, Cambridge University Press, 2000.
[33] A.T. Petit, P.L. Dulong, Ann. Chim. Phys. 10 (1819) 395.
[34] V. Krasnenko, M.G. Brik, Solid State Sci. 14 (2012) 1431.